Heterometallic coordination polymers based on CuII/LnIII cations. Solid-state and magnetic characterization

B. Baldo, T. Bataille, D. Venegas-Yazigi, Nathalie Audebrand, V. Paredes-García

Heterometallic coordination polymers based on Cu^{II}/Ln^{III} cations. Solid-state and magnetic characterization

*Bianca Baldo,[a,b] Thierry Bataille,[b] Diego Venegas-Yazigi,[c,d] Nathalie Audebrand[*b] and Verónica Paredes-García[*a,d]*

[a.] Universidad Andres Bello, Departamento de Ciencias Químicas, Santiago, Chile.

[b.] Univ Rennes, Ecole Nationale Supérieure de Chimie de Rennes, CNRS, ISCR (Institut des Sciences Chimiques de Rennes) - UMR 6226, F-35000 Rennes, France.

[c.] Universidad de Santiago, Departamento de Química de los Materiales, Santiago, Chile.

[d.] CEDENNA, Santiago, Chile.

* Correspondence: nathalie.audebrand@univ-rennes1.fr; vparedes@unab.cl

This manuscript is dedicated to Professor Jean René Hamon on the occasion of his 65th birthday.

KEYWORDS. Heterometallic Coordination Polymers, Cu-Ln-Networks, Structural Characterization, Magnetic Properties, Ultrasound synthesis, Sonochemistry.

ABSTRACT

Novel heterometallic three-dimensional coordination polymers $\{[Cu^{II}_2Ln^{III}Cl_2(HIA)_4(NO_3)(DMF)_2]\cdot(2DMF)\cdot(H_2O)\}_n$ based on Ce (**1**), Eu (**2**) or Gd (**3**) and imidazole-4-acrylic acid (H_2IA), were successfully synthesized using the sonochemical method. All attempts to obtain the compound using other synthetic methods were unsuccessful. The heterometallic polymers are isostructural, crystallizing in the chiral *P3₂21* trigonal space group. The crystal structures are characterized by an intricated 3D framework that can be rationalized in terms of $Cu(HIA)_2$ fragments that generate two interpenetrated copper(II) networks, $[Cu(HIA)_2]_n$, which are also connected by the interaction of the Ln^{III} cations with the carboxylate group belonging to the organic ligand, thus conferring a higher complexity to the 3D network. Additionally, the coordination environment around the copper(II) cations is responsible for the chirality of the structures, making these even more exciting. The three-dimensional polymers were also characterized from a magnetic point of view, obtaining for (**1**) and (**2**) antiferromagnetic interactions, while for (**3**) ferromagnetic interactions were observed. Furthermore, to the best of our knowledge, these coordination polymers are the first heterometallic compounds based on *3d/4f* cations, assembled by the ligand imidazole-4-acrylate (HIA^-).

1. INTRODUCTION

During the last years, the interest in the synthesis of heterometallic coordination polymers based on transition metals and lanthanide cations have proved to be attractive not only by their peculiar electronic properties but also by the applications in different areas, such as magnetism, luminescence, gas sorption, non-linear optics, among others. [1-7] Several synthesis methods have

been used to prepare coordination polymers. However, the hydro/solvothermal and conventional solution methods are the most commonly reported in the literature.[8,9] In the last few years microwave-assisted, electrochemical, mechanochemical and sonochemical methods have also emerged as successful routes to synthesize coordination polymers, mainly due to the required short time involved in this type of processes.[7-10] Precisely, the sonosynthesis consists of applying ultrasound waves to produce a cavitation phenomenon that means formation, growth and subsequent collapse of microbubbles, which release a large magnitude of energy inducing localized extreme conditions.[8,11] This method has been mainly applied in the organic synthesis and to prepare metallic nanoparticles [12-14] and has only been recently reported to synthesize coordination polymers.[15,16] For instance, $[Zn_3(BTC)_2]_n \cdot 12H_2O$, $[Zn(BDC)(H_2O)]_n$, $[Cd_2(BTC)_2(H_2O)_2]_n$, $[Co_3(BTC)_2]_n$ are examples of coordination polymers based on transition metal cations synthesized using sonosynthesis.[17-20] In contrast, examples based on *4f* cations are scarce, but also can be mentioned $[Ce(BTC)(H_2O) \cdot 4.3H_2O]_n$, $[Tb(BTC)(H_2O) \cdot 4.3H_2O]_n$ and $[Ce(BTC)(H_2O)_6]_n$.[21,22] It is important to note that the examples mentioned above correspond to homometallic coordination polymers based on metal cations (*nd* or *4f*) and organic ligands containing carboxylate groups. Therefore, to consider the sonosynthesis as an exciting method to prepare novel heterometallic coordination polymers, it is also necessary to choose an appropriate ligand to have the assembly in the same structure of both *3d* and *4f* cations. In our case, the choice of the imidazole-4-acrylic acid (H_2IA) as a ligand was done, considering that it possesses N and O atoms, necessary to bind *3d* and *4f* cations, respectively.[23] Furthermore, the rotation of the imidazolyl ring and the H transfer between the two N atoms can generate multiple tautomeric species,[24] giving to the H_2IA ligand excellent coordination capabilities to obtain coordination polymers with new architectures and expected new properties.[25,26] Additionally, to the best of

our knowledge, *3d/4f*-heterometallic coordination polymers based on the ligand imidazole-4-acrylic acid (H_2IA) have not been reported up to date in the literature, making this ligand even more attractive. Therefore in this work, together with reporting the use of sonosynthesis as an effective method to prepare *3d/4f*-heterometallic networks, we are also reporting the first examples of chiral 3D-networks, based on the cations Cu^{II}, Ln^{III} and the H_2IA ligand, namely $\{[Cu^{II}_2Ln^{III}Cl_2(HIA)_4(NO_3)(DMF)_2]\cdot(2DMF)\cdot(H_2O)\}_n$, (Ln= Ce (**1**), Eu (**2**), Gd (**3**)), which were characterized from a structural and magnetic viewpoint.

2. MATERIAL AND METHODS

2.1 Synthetic procedure

Heterometallic coordination polymers can be synthesized using different synthetic methods that include bench conditions, solvo/hydrothermal conditions, and mechanochemical or sonochemical routes. However, in our case all attempts to obtain heterometallic coordination polymers using bench synthesis or hydro/solvothermal conditions at different temperatures, molar ratios, and solvents were unsuccessful when the imidazole-4-acrylate (HIA^-), an appropriate linker to bind *3d* and *4f* cations, was used. We also tried the mechanochemical method but without successful results. In all cases, only 3*d*-homometallic molecular systems were obtained. The sonochemical route was the only synthetic method capable of producing the appropriate conditions to obtain the *3d-4f*-heterometallic coordination polymers presented in this study. All reagents and solvents were of P.A. quality and used without any previous purification process. The syntheses were performed using a Qsonica Sonicator model Q500.

2.2 Synthesis of $\{[Cu^{II}_2Ln^{III}Cl_2(HIA)_4(NO_3)(DMF)_2]\cdot(2DMF)\cdot(H_2O)\}_n$, Ln^{III}=Ce(**1**), Eu(**2**), Gd(**3**)

Synthesis of (**1**): In a Teflon vessel was prepared a mixture of $CuCl_2 \cdot 2H_2O$ (0.085 g, 0.5 mmol), $Ce(NO_3)_3 \cdot 6H_2O$ (0.217 g, 0.5 mmol) and H_2IA (0.069 g, 0.5 mmol) with 10 mL of N,N'-dimethylformamide (DMF). This mixture was sonicated continually for 10 minutes at room temperature with ultrasonic power of 500 W, 20 kHz of frequency, and 25 % of amplitude, leading to a green colour solution, which was then left at room temperature by one month until some blue-greenish prism crystals appear. The syntheses of (**2**) and (**3**) were carried out under similar conditions than (**1**), but using $Eu(NO_3)_3 \cdot 5H_2O$ (0.214 g, 0.5 mmol) and $Gd(NO_3)_3 \cdot 6H_2O$ (0.226g, 0.5 mmol) in case of (**2**) and (**3**), respectively.

2.3 Characterization

Crystal structure Determination. Single-crystal X-ray diffraction data of the compounds (**1**), (**2**), (**3**) were collected at 150 K on a D8 VENTURE Bruker AXS diffractometer and processed with the APEX3 [27] program suite. The X-ray wavelength used was Mo-K_α (λ = 0.71073 Å). Frame integration and data reduction were carried out with the program SAINT.[28] The program SADABS [29] was employed for multiscan-type absorption corrections. The structures were determined by a dual space algorithm using the SHELXT [30] program, and the structural models were then refined with full-matrix least-squares methods based on F^2 (SHELXL program)[31] with the aid of the OLEX2 package.[32] Crystallographic data, details on data collections and refinement parameters of the crystal structures are given in Table S1. Structure drawings have been made with DIAMOND [33] and ORTEP [34] programs. SHAPE [35] program was used to determine the coordination geometry and symmetry of the different cations. The purity of the phases was checked by X-ray powder diffraction, also investigating the thermal stability of (**1**), (**2**), (**3**) between 25 and 800 °C. TGA-DSC measurements of ground crystals were performed on an SDT Q600 thermal analysis equipment under a N_2 atmosphere with a heating rate of 1°C/min

until 250 °C and 5 °C/min until 800 °C. In situ X-ray powder diffraction measurements were performed within an Anton Paar HTK 1200N chamber under N_2 atmosphere attached to a Panalytical Empyrean powder diffractometer (θ–θ Bragg–Brentano geometry) working with the Cu-Kα radiation (λ $K\alpha_1$ = 1.5406 Å, λ $K\alpha_2$ = 1.5444 Å) selected with a flat multilayer X-ray mirror (Bragg-Brentano HD®). Data were collected with a Pixel 1D silicon-strip detector in the useful angular range. Powder patterns were collected every 5 °C, between 5 and 61° 2Θ.

Magnetic Susceptibility. Magnetic measurements were performed on polycrystalline samples and carried out using a Quantum Design Dynacool Physical Properties Measurement System (PPMS) equipped with a vibrating sample magnetometer (VSM). The *dc* data were collected under an external applied field of 1.0 kOe and 10.0 kOe in the 1.8−300 K temperature range. Diamagnetic corrections (estimated from Pascal constants) were considered. [36] Magnetization measurements were performed between 0 and +90 kOe at temperatures of 1.8, 3, 5 and 8 K. The dynamic *ac* susceptibility data were collected in the 1.8−11 K range with *dc* field of 5.0 kOe, at frequencies between 100 and 10000 Hz using 1 or 4 Oe of oscillating field.

Spectroscopic Measurements. FTIR spectra were recorded on a Bruker Equinox 55 spectrophotometer in the 4000–400 cm^{-1} range, using KBr pellets. UV–Vis-NIR spectra were obtained on a Perkin Elmer Lambda 650 spectrophotometer UV–Vis/NIR, equipped with a Spectralon 60 mm InGaAs Integrating sphere. The measurements were carried out in the 200–850 nm range using the solid sample without any support.

3. RESULTS AND DISCUSSION

3.1 Structural Description

The structure determination from the single-crystal X-ray diffraction data shows that the heterometallic networks of (**1**), (**2**) and (**3**) are isostructural, crystallizing in the chiral trigonal $P3_221$ space group (Table 1 and S1). Three-dimensional networks of (**1**), (**2**) and (**3**) are generated by the coordination of the monoprotonated ligand (HIA^-) to the Cu^{II} and Ln^{III} cations. In the structures of (**1**)-(**3**), the organic ligand appears as imidazole-5-acrylate due to a tautomeric conversion that the initial reagent, imidazole-4-acrylic acid, can present, as shown in Scheme 1.

This tautomeric conversion has also been observed in homometallic coordination polymers based on the same organic ligand, like $\{[Cu(1)_3Cu(2)(HIA)_6](SO_4)\}_n \cdot nH_2O$ and $\{[Cd(HIA)_2](H_2O)_{3/2}(EtOH)\}_n$, reported by Y. Xu et al., [25] and R.-Q. Zou et al., [26]

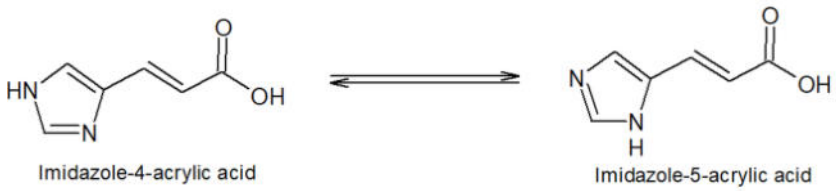

respectively.

Scheme 1. Tautomerisation of imidazole-4-acrylic acid into imidazole-5- acrylic acid.

The crystal structures of (**1**), (**2**) and (**3**), are characterized by one crystallographic independent lanthanide atom and one crystallographic independent Cu atom. The Cu^{II} cations have a five-coordination environment with a square pyramidal geometry ($CuClN_2O_2$, C_{2v}), generated by the binding of four HIA^- and one chloride anion. The HIA^- anions are disposed in the basal plane of the pyramid, coordinating the Cu cation for two of them through one oxygen atom belonging to the carboxylate group, and for the other two ligands through nitrogen atoms from the imidazole ring. The chloride anion is localized in the axial position, completing the coordination sphere around the Cu^{II} cation (Figure 1a) with a Cu-Cl bond length close to 2.5 Å, while the Cu-O and

Cu-N distances are close to 2.0 Å and 1.9 Å, respectively (Table S2). It is important to remark that the Cu-Cl distances in these compounds are slightly higher than those reported in the literature for similar systems [37-39], usually in the range of 2.2 to 2.4 Å. Another peculiarity of the structure is its chirality, which is reached by the spatial position of the HIA^- ligands around the Cu cation. On the other hand, the Ln^{III} cations are surrounded only by the oxygen atoms belonging to four molecules of monoprotonated ligands (HIA^-), one chelating nitrate anion which presents disorder (half occupancy on N1 and O2 atoms) and two DMF molecules, reaching a LnO8 arrangement with a dodecahedron geometry (D_{2d}, Figure 1b). As shown in Table S2, the Ln-O1 distances, with O1 oxygen atom belonging to the disordered nitrate anion, are around 2.6 Å for (**1**) and 2.5 Å for (**2**) and (**3**). Similarly, the Ln-O3 distances, with O3 oxygen atom belonging to DMF molecules (Ln-O3), are close to 2.5 Å for (**1**) and 2.4 Å for (**2**) and (**3**). The same trend is observed for the Ln-O distances involving O atoms belonging to HIA^- species (O4 and O6) with values around 2.4 Å for (**1**) and 2.3 Å for (**2**) and (**3**). These distances are in agreement with the Ln-O distances reported for the analogous compound, $[Ln^{III}Cu^{II}(MA)_4(H_2O)_4]_n(MA)_n$, (MA= α- metacrylate), which contain an organic ligand also functionalized with carboxylate group and the same Ln^{III} cations (Ce, Eu and Gd).[40] In compounds (**1**), (**2**) and (**3**) the monoprotonated organic HIA^- species is acting as a tridentate ligand (imidazole-4-acrylate-κ^3O',O'',N), connecting both Cu^{II} and Ln^{III} cations by means of the carboxylate groups and the imidazole ring (Figure 2a). This coordination of the ligand HIA^- to Cu^{II} and Ln^{III} cations gives rise to an intricated 3D framework (Figure 2b). The structures can be described from trimers units built by two copper and one lanthanide cations (Figure 3), each trimer being interconnected by the ligands, thus forming the network.

Alternatively, the network can be rationalized in terms of 2-fold interpenetrated networks constituted by two distinct chains based on $[Cu(HIA)_2]$ units, as shown in Figure 4a. Within each chain, the ligand bridges two copper cations with $Cu^{II}\cdots Cu^{II}$ distances (Cu-HIA-Cu, Figure S1a) of 10.7574(11), 10.7679(16) and 10.7509(12) Å, for (**1**), (**2**) and (**3**), respectively. The copper-based chains are connected one through the coordination of the Ln^{III} cations with the carboxylate groups belonging to the $[Cu(HIA)_2]_n$ chains (Figure 4b). The shortest $Cu^{II}\cdots Ln^{III}$ distance is obtained by the *syn-anti* coordination mode of the carboxylate group to both cations (Cu^{II}-OCO-Ln^{III}, Figure S1b), leading to values of 4.2361(7), 4.2007(12) and 4.1888(14) Å for (**1**), (**2**) and (**3**), respectively while the longest $Cu^{II}\cdots Ln^{III}$ distances that involves the imidazole ring and the carboxylate group of the HIA^- anions (Figure S1c) give values of 9.0290(9), 9.0456(15) and 9.0355(10) Å, for (**1**), (**2**) and (**3**), respectively. In the same way, $Cu^{II}\cdots Cu^{II}$ distances of 7.0406(17) Å, 7.049(2) Å and 7.031(2) Å, for (**1**), (**2**) and (**3**), respectively can be found considering the following bridge Cu^{II}-COO-Ln^{III}-OCO-Cu^{II} (Figure S1d). Table S3 shows the most important interatomic distances for Cu^{II}/Ln^{III} cations. It is important to note that only a few examples of coordination polymers based on the ligand imidazole-4-acrylic acid are reported in the literature. In all cases the authors report three-dimensional homometallic networks based on Zn^{2+} or Cd^{2+} like in $[Cd(HIA)_2\cdot 1.7H_2O]_n$, $\{[Cd(HIA)_2(H_2O)_{3/2}(EtOH)\}_n$, $\{[Zn(HIA)_2](H_2O)_{4,25}\}_n$ and $\{[Zn(HIA)_2]H_2O\}_n$. [26,41-43] In the reported structures, the *nd* cations are also surrounded by four monoprotonated ligands (HIA^-), which are coordinating in the same way that the compounds reported in this work. However, the units of $[Cu(HIA)_2]_n$ present in (**1**), (**2**) and (**3**) give rise to two interpenetrated networks, while the homometallic compounds reported in the literature give four- and five-fold interpenetrated networks. This fact permits us to infer that probably the HIA^- ligand reacts first with the *3d* cation producing growth of the $[Cu(HIA)_2]_n$, which is directed by the coordinative capabilities of the

organic ligand and the coordination versatility from the transition metal. Later the coordination of the Ln^{3+} cations to the carboxylate groups should prevent additional interpenetrations of the networks. Then, considering the structural features of the heterometallic networks, the calculated voids in a lattice represent only 23 % for (**1**) and 24 % for (**2**) and (**3**), with empty channels along the c axis (Ø ~ 3.6 Å, Figure S2). The crystallization solvent molecules of water and N,N'-dimethylformamide are localized in the voids, close to the ligands, giving rise to hydrogen bonds as a product of the interaction between the O atoms (O8A and O8B) of the DMF molecules and H atoms (N4-H4) of the imidazole ring (Table S4). The solvent molecules present disorder of the hydrogen atoms of water molecules (half occupancy of H10A and H10B linked to O10). Remarkably, no heterometallic compound based on Cu^{II}-Ce^{III}, Cu^{II}-Eu^{III} or Cu^{II}-Gd^{III} assembled by the H_2IA ligand was found in the Cambridge Structural Database.[44] However, a family of one-dimensional coordination polymers also based on the Cu^{II}-Ln^{III} cations, but using α-metacrylic acid (HMA) as ligand, $[Ln^{III}Cu^{II}(MA)_4(H_2O)_4]_n(MA)_n$, has been reported by F. Chen and co-workers.[40] In this family, the carboxylate group acts as a bridge between the two kinds of cations, with a syn-anti disposition, similar to the compounds reported in this work. The Cu-Ln distances given by the authors are 3.88 Å for Cu-Ce and 3.83 Å for Cu-Eu and Cu-Gd, which are lower than those observed for (**1**), (**2**) and (**3**) for an equivalent bridge. The authors also report that the bridge generated by the carboxylate group permits magnetic interactions between the Cu^{II} and Ln^{III} cations. Then, magnetic interactions are also expected for the compounds (**1**), (**2**) and (**3**).

3.2 Thermal, spectroscopic and magnetic properties

Thermal Stability. In addition to the single-crystal X-ray diffraction, the purity of the three phases was confirmed by powder X-ray diffraction, in which the experimental patterns are in good agreement with the simulated patterns obtained from the single-crystal data (Figure S3). It is

important to notice that the broad line at low angles observed in experimental PXRD is due to the diffuse scattering of the heating chamber. The thermal stability of the single-phase polycrystalline samples (**1**-**3**) was evaluated between 20 and 900 °C under a nitrogen atmosphere (Figure S4). In the studied temperature range, the thermograms show that multistep weight losses processes characterize the three compounds. The first significant weight losses are obtained around 130 ºC with values of 13.45, 9.20 and 13.50 wt% for (**1**), (**2**) and (**3**), respectively, associated with the release of the crystallization solvent molecules. The obtained values can be correlated with those calculated considering two DMF and one water molecules ((**1**): 13.06; (**2**): 12.94 and (**3**): 12.89 wt%). Discrepancies between the calculated and observed values could be explained by different amount of crystallization solvent molecules in the starting compositions. A decrease of 19.60, 16.10 ad 17.20 wt% was observed for (**1**), (**2**) and (**3**) between 130 and 250 ºC, correlated with the loss of two coordinated DMF molecules and one nitrate anion (calculated values: (**1**) = 16.57 %; (**2**) = 16.41 % and (**3**)= 16.34 %), thus producing the structural collapse.

Structural modifications as a function of the temperature were corroborated by X-ray powder diffraction technique (Figure 5 and S5). The obtained powder diffraction patterns show that the pristine structures are preserved without loss of crystallinity until c.a. 130 °C for (**1**) and (**3**) and 140°C for (**2**). From 130 ºC, the diffraction patterns show significant changes indicating that chemical transformations occur. Amorphous phases are obtained in the range of 220-580 ºC for (**1**); 220-650 ºC for (**2**) and 220-670 ºC for (**3**). Finally, new peaks associated to the presence of CeO_2-Cu-Cu_2O or Eu_2O_3-Cu-Cu_2O or Gd_2O_3-Cu-Cu_2O cubic phases are observed at temperatures higher than 580, 650 and 670 °C for (**1**), (**2**) and (**3**), respectively. One can notice that during the thermal decomposition under N_2, reduction of Cu^{II} into Cu^{I} or Cu^{0} occurs.

Spectroscopic Properties. FTIR spectra of (**1**), (**2**), (**3**) and the free ligands are given in the supplementary material (Figure S6). The FTIR spectra of (**1**), (**2**) and (**3**) are very similar, agreeing with the reported for one analogous system.[45] Broad absorptions characterize the spectra at 3400 cm^{-1} and 3150 cm^{-1} assigned to O-H and N-H stretching vibration belonging to water and imidazole ring, respectively. Absorptions associated with asymmetric ($\bar{\upsilon}_{COOa}$) and symmetric ($\bar{\upsilon}_{COOs}$) vibrations of the carboxylate groups appear in the region 1540-1430 cm^{-1}. The bands associated with the C=C bond and the imidazole ring appear at 1650 cm^{-1} and 1355 cm^{-1}. The strong absorption at 1380 cm^{-1} is indicative of the ionic character of the interaction between NO_3^- anion and Ln^{III} cation.

The solid UV-vis spectra obtained for the free ligand (H_2IA) and (**1**), (**2**) and (**3**), are given in Figure S7. As expected, similar electronic spectra were obtained for heterometallic networks, being dominated by the intense absorptions belonging to the organic fragment at 260 nm and 320 nm associated to π-π* and n-π* transitions,[19] respectively. The broad absorption at 500 nm was assigned *to d→d* transitions, concordant with reported other Cu^{II} cations with a similar coordination environment.[46,47] On the other hand, (**1**), (**2)** and (**3**) were excited at 330, 350 and 370 nm, respectively, but no emission was observed. This phenomenon can be explained considering that Cu^{II} cations should quench the luminescence process centered on the interactions of the organic ligand and the lanthanide cations together to coordinate solvent molecules that should also contribute to having a non-radiative relaxation process. [48,49]

Magnetic Properties. The dc magnetic measurements of (**1**), (**2**) and (**3**) were performed as a function of magnetic field and temperature. The reduced magnetization Nβ of (**1**), (**2**) and (**3**) at four different temperatures shows the lack of overlap of the Nβ vs. HT^{-1} plots of (**1**) and (**2**), suggesting the presence of magnetic anisotropy (Figure 6). Besides, the saturation is not entirely

reached at 1.8 K even at the maximum applied field of 90 kOe, giving values of 2.9 and 2.5Nβ for (**1**) and (**2**), respectively. In the case of (**1**) the value is much smaller than the expected saturation magnetization (M_s) value of 4.1Nβ for non-interacting $CeCu_2$ core (J=5/2, g=6/7 for Ce^{III} and g=2.0 and S=1/2 for Cu^{II} cations). However, for (**2**) it is higher than the value expected of 2Nβ for non-interacting $EuCu_2$ core (J=0 and g_j=0 for Eu^{III} cation and S=1/2 for Cu^{II} cations). On the contrary, compound (**3**) shows a complete overlap of the curves confirming the lack of first-order orbital moment contribution as expected for the isotropic Gd^{III} cation. Furthermore, at 1.8 K the saturation is reached at 60 kOe giving a value of 9.2Nβ, which is close to the calculated saturation magnetization (M_s) value of 9Nβ, expected for non-interacting $GdCu_2$ core (g=2.0 and S=7/2 for Gd^{III} cation; S=1/2 for Cu^{II} cations).

The temperature dependence of the magnetic susceptibility was obtained in the 1.8-300 K range under an applied field of 1 kOe and 10 kOe. For (**1**) and (**2**) similar behaviors are observed at both applied fields (Figure 6 and 7). The results at 1 kOe for (**1**), (**2**) and (**3**) are plotted as $\chi_m T$ product vs. T in Figure 6. At 300 K, $\chi_m T$ values of 1.57, 2.46 and 8.50 cm^3Kmol^{-1} are obtained for (**1**), (**2**) and (**3**), respectively. Only in the case of (**1**) and (**3**), the obtained $\chi_m T$ values are comparable with the expected ones for one Ln^{III} and two Cu^{II} non-interacting cations ($LnCu_2$), i.e., 1.55 cm^3Kmol^{-1} for (**1**) and 8.63 cm^3Kmol^{-1} for (**3**) (Ce: $^2F_{5/2}$, g_j=6/7 ; Gd: $^8S_{7/2}$, g=2.0 and Cu^{II}: g=2.0).[50] For (**2**), the $\chi_m T$ value at room temperature is higher than the expected one for a non-interacting $EuCu_2$ core, (0.75 cm^3Kmol^{-1}, $^7F_0$, g_j=0 for Eu^{III} and S=1/2 for Cu^{II} cations). Specifically, the Eu^{III} ion has a $^7F_0$ ground state and the two nearest excited states are $^7F_1$ at *ca*. 350 cm^{-1} and $^7F_2$ at ca. 1000 cm^{-1}, respectively. Therefore, at room temperature the excited states are populated, explaining in this form the higher experimental $\chi_m T$ obtained value for **(**2).[51] Upon cooling $\chi_m T$ values decrease continuously for (**1**) and (**2**) reaching values 1.09 cm^3Kmol^{-1} at 10 K for (**1**) and 0.95

cm^3Kmol^{-1} at 13 K for (**2**). A more abrupt decrease is observed at lower temperatures for both compounds giving at 1.8 K χ_mT values of 0.88 and 0.64 cm^3Kmol^{-1} for (**1**) and (**2**), respectively. For (**1**), the decrease of χ_mT on lowering the temperature is likely due to depopulation of the M_J sublevels of the anisotropic Ce^{III} cation arising from the splitting of the ground term by the ligand field (Stark Levels), while for (**2**) it can be attributed to the depopulation of the excited states. The phenomenon observed at the low range of temperature can be rationalized as a weak antiferromagnetic interaction present in compounds (**1**) and (**2**). Compound (**3**) has a χ_mT value, which remains practically unchanged until 50 K (8.52 cm^3Kmol^{-1}). Below 50 K, an increase of the χ_mT value can be observed, presenting a maximum of 9.47 cm^3Kmol^{-1} at 2 K, suggesting ferromagnetic Cu-Gd interaction in the network. Below this temperature, the χ_mT decreases again reaching a value of 9.40 cm^3Kmol^{-1} at 1.8 K. A similar behavior is observed at 10 kOe for (**3**), but with a maximum of 8.64 cm^3Kmol^{-1} that appears at 9.5 K. From this temperature, the χ_mT shows a sharp decrease reaching a value of 6.36 cm^3Kmol^{-1} at 1.8 K (Figure 7).

On the other hand, alternating current (*ac*) magnetic susceptibility measurements were performed using 1 or 4 Oe of an oscillating field in the frequency range of 1000 and 10000 Hz. In the absence of an external dc field, the dynamic magnetic measurement data do not present maximum, but if a *dc* field of 5000 Oe is applied, a well-defined maximum at 6 K was observed for the out-of-phase (χ'') for all studied frequencies (Figure S8b), confirming the existence of ferromagnetic behavior in this region.[52-54] Moreover, both the in-phase (χ') and out-of-phase (χ'') the maxima positions are frequency independent (Figure S8). Taking into account the isotropic character of Gd^{III} cation, a spin-only formalism can be applied to characterize the magnetic behavior in (**3**). Then, a trinuclear small fragment Cu-Gd-Cu (Figure 3) was taken as a

model to fit the experimental magnetic susceptibility data. According to the proposed model, the exchange magnetic coupling between Cu^{II} and Gd^{III} cations can be described by the following spin Hamiltonian:[55-57]

$$\mathcal{H} = -J(S_{Cu1} + S_{Cu2})S_{Gd} \qquad \text{(eq. 1)}$$

The experimental magnetic susceptibility data of (**3**) obtained between 300 and 1.8 K were fitted using the following expression.[49]

$$\chi T = \left(\frac{Ng^2{\mu_B}^2}{2k_B}\right)\left[\frac{\left(35+84e^{\left(\frac{9J}{2k_BT}\right)}+e^{\left(\frac{7J}{2k_BT}\right)}+165e^{\left(\frac{8J}{k_BT}\right)}\right)}{\left(6+8e^{\left(\frac{9J}{2k_BT}\right)}+e^{\left(\frac{7J}{2k_BT}\right)}+10e^{\left(\frac{8J}{k_BT}\right)}\right)}\right] \qquad \text{(eq. 2)}$$

The best results were obtained with a J_{GdCu} value of 0.58 cm^{-1}, and considering $g_{Gd}=g_{Cu}=2.00$. Introducing a ZJ= -0.35 K it was possible to reproduce the decrease of $\chi_m T$ at 1.8 K and modelling very well the magnetic behavior observed for compound (**3**) ($R=1\cdot10^{-5}$, Figure S9). The exchange coupling parameter obtained for compound (**3**), is lower than the observed one for the similar network $[Gd^{III}Cu^{II}(MA)_4(H_2O)_4]_n(MA)_n$,[40] where the authors report a J value of 2.62 cm^{-1} for $Cu^{II}Gd^{III}$ dimers which are bonded through the bridges generated by the carboxylate groups and with a distance of 3.83 Å between them. Also, Kahn and co-workers.[54,58] proposed a correlation between the lanthanide cation and the magnetic behavior of the compounds based on Cu^{II}-Ln^{III} cations. Thus, antiferromagnetic interaction is expected for compounds based on Ln^{III} ions with less than seven *4f* electrons and ferromagnetic interaction otherwise. Therefore, it can be expected that a ferromagnetic interaction is obtained for both copper centers with the gadolinium ion in each trinuclear unit.

In summary, compound (**3**) can be described as a network formed by weak ferromagnetic trinuclear units, which are canted and disposed of antiparallel in the network, thus producing an antiferromagnetic response at lower temperatures when the low dc external field is applied. However, when a stronger dc external field is applied, the canted 9/2 trinuclear spins are perfectly antiparallel aligned; thus an antiferromagnetic phenomenon is observed (Figure 7). A plot of ln (χ''/χ') vs. 1/T does not give parallel lines for the high-frequency measurements indicating that no slow relaxation of the magnetization process is present in each ferromagnetic trinuclear unit, which is clearly due to the presence of the neighboring units, which are helping in the relaxation process, i.e. the trinuclear units are not magnetically isolated.

4. CONCLUSIONS

In summary, a new family of Cu^{II}/Ln^{III} chiral heterometallic coordination polymers based on the ligand imidazole-4-acrylic acid (H_2IA) was only possible to obtain using the sonochemical synthesis route. All attempts using other synthetic methods gave 3*d*-homometallic molecular systems. The 3D structures $\{[Cu_2Ln(NO_3)Cl_2(HIA)_4(DMF)_2]\cdot(2DMF)(H_2O)\}_n$ can be rationalized, on the one hand, in terms of two substructures constituted by $[Cu(HIA)_2]_n$ fragments which are also part of 2-fold interpenetrated networks bonded by Ln^{III} cations and, on the other hand, from trimers of Cu^{II} and Ln^{III} cations. From a magnetic point of view, beyond the intrinsic magnetic characteristics of the lanthanide cations, the networks reported in this work are characterized by a paramagnetic behavior presenting weak interactions only perceptible at low temperatures. Thus, antiferromagnetic interactions below 10 K could be present in Cu^{II}/Ce^{III} (**1**) and Cu^{II}/Eu^{III} (**2**), while a weak ferromagnetic interaction is present in Cu^{II}/Gd^{III} (**3**) below 50 K. The ferromagnetic trinuclear units are antiparallel ordered and canted in the solid, giving bulk antiferromagnetic behavior in the lowest temperature range.

FIGURES

Figure captions

Figure 1. Heterometallic compound $\{[Cu^{II}_2Ce^{III}Cl_2(HIA)_4(NO_3)(DMF)_2]\cdot(2DMF)\cdot(H_2O)\}_n$. Coordination environment of (a) Cu^{2+} cation and (b) Ln^{3+} cation.

Figure 2. Coordination polymer $\{[Cu^{II}_2Ce^{III}Cl_2(HIA)_4(NO_3)(DMF)_2]\cdot(2DMF)\cdot(H_2O)\}_n$. (a) Detail of the heterometallic network.; (b) Projection along a axis of the unit cell of the 3D-network.

Figure 3. Detail of the structure of the 3D network enhancing the trimers based on Cu^{II} and Ce^{III} cations.

Figure 4. (a) Detail of the interpenetrated $[Cu(HIA)_2]_n$ networks bonded by Ln^{3+} cations; (b) Projection along b axis of the unit cell of the 3D-interpenetrated networks.

Figure 5. Thermal stability of compound (**1**) under N_2 atmosphere. (a) Powder X-ray diffraction patterns as a function of temperature; (b) Highlight of the first part of the decomposition process.

Figure 6. Variable temperature magnetic susceptibility of (a) Cu^{II}/Ce^{III} (**1**); (b) Cu^{II}/Eu^{III} (**2**); (c) Cu^{II}/Gd^{III} (**3**) at 1 kOe. Inset shows the 1.8−8.0 K field-dependent magnetization.

Figure 7. Variable temperature magnetic susceptibility of Cu^{II}/Ce^{III} (1); Cu^{II}/Eu^{III} (2) and Cu^{II}/Gd^{III} (**3**) at 10 kOe.

a

b

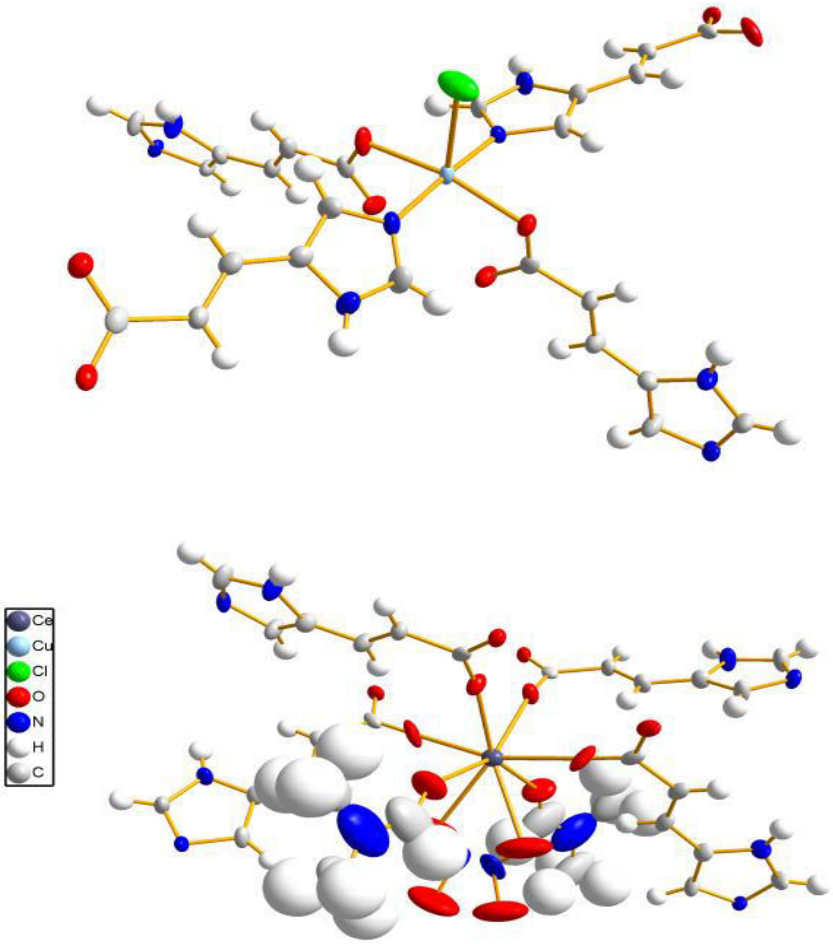

Figure 1

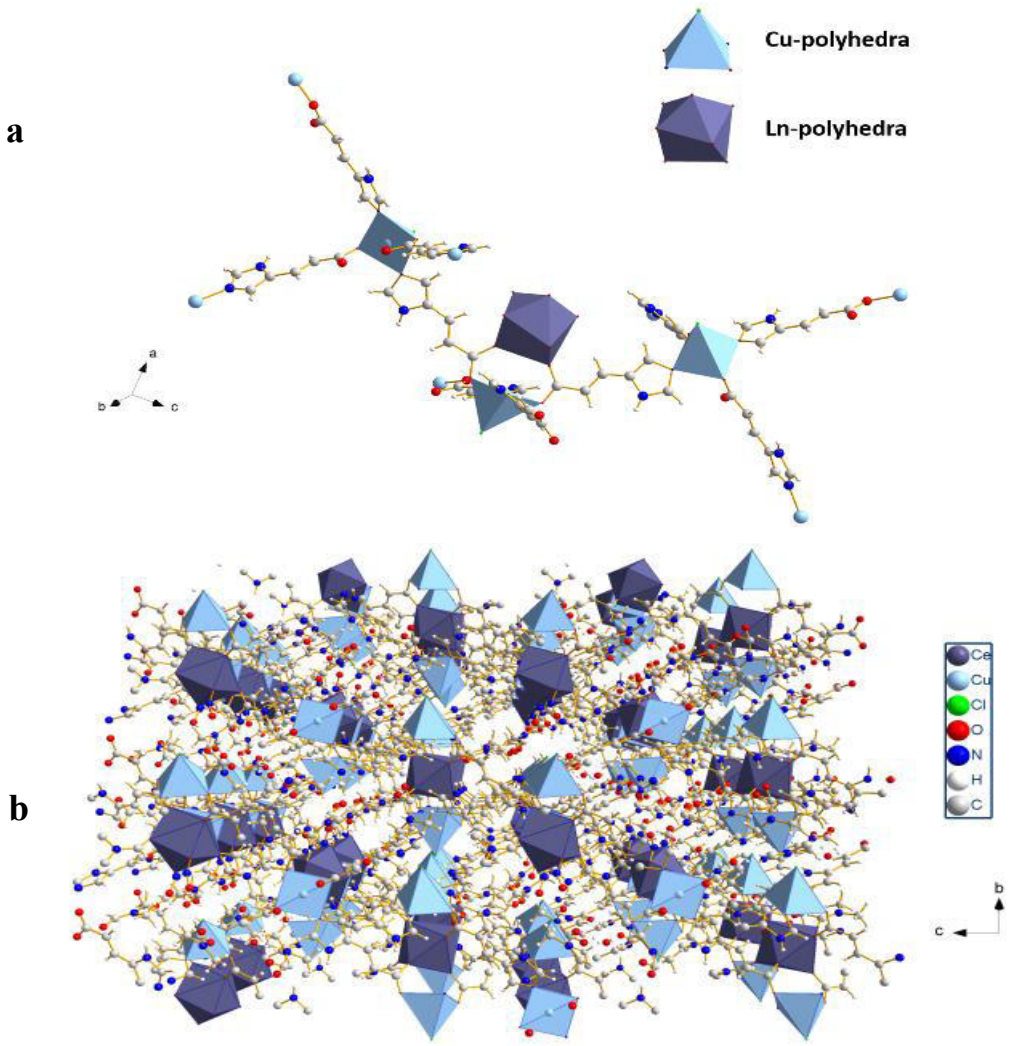

Figure 2

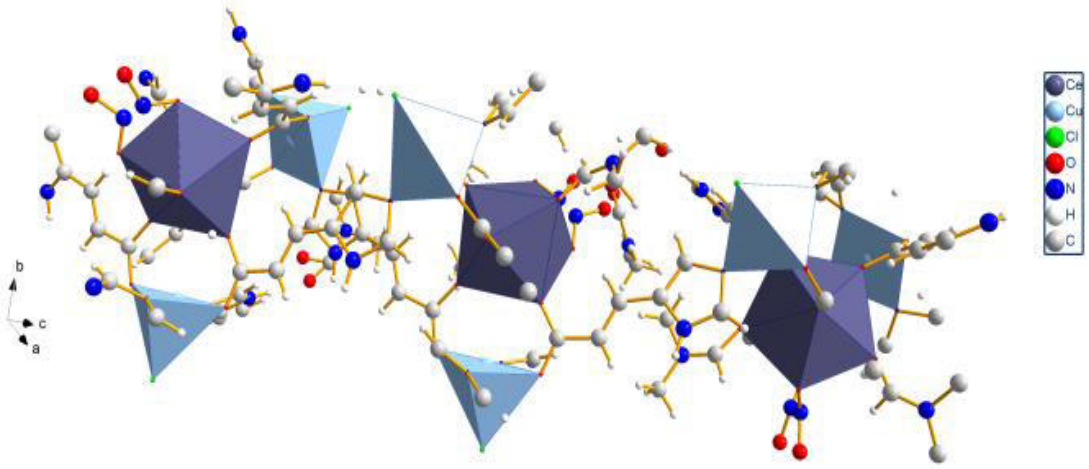

Figure 3

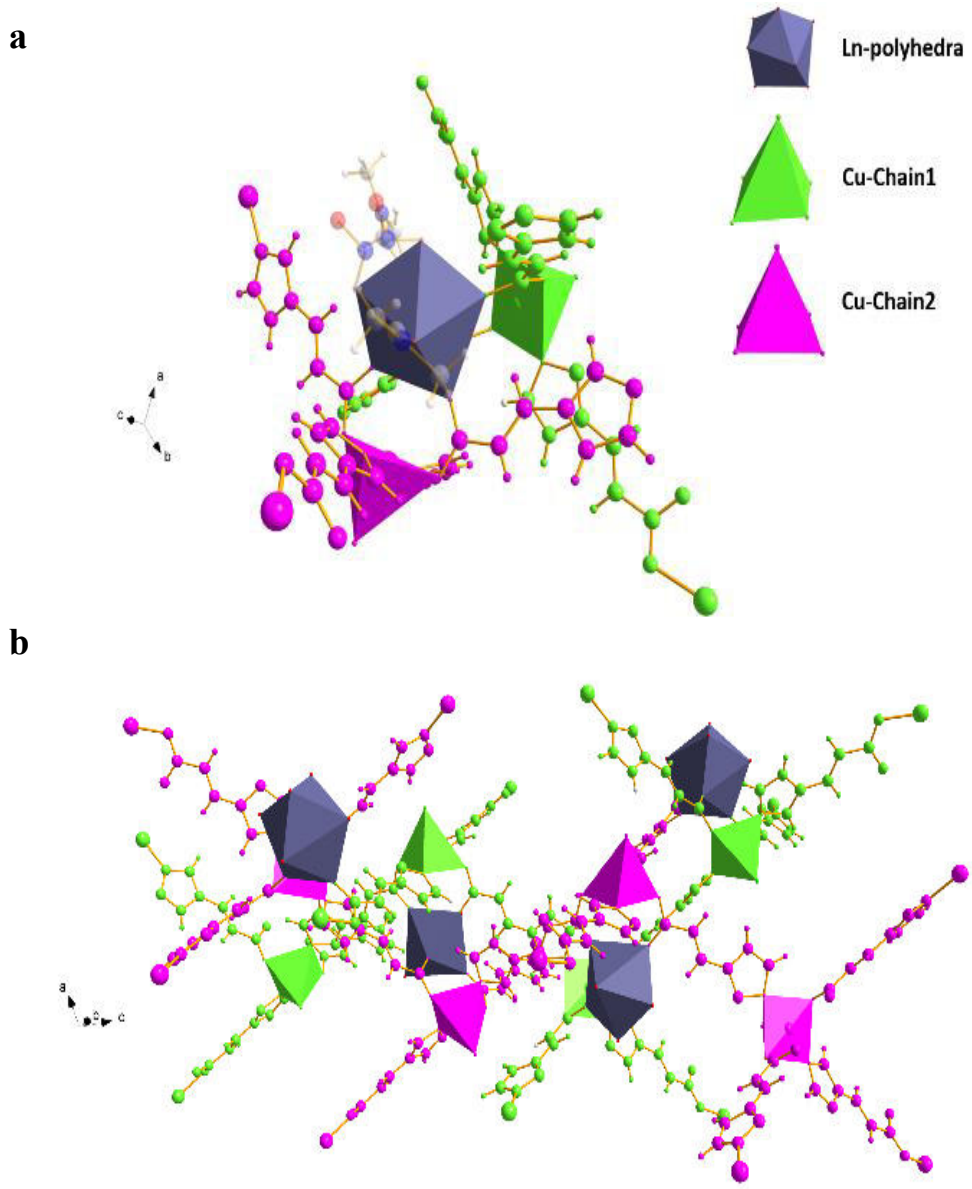

Figure 4

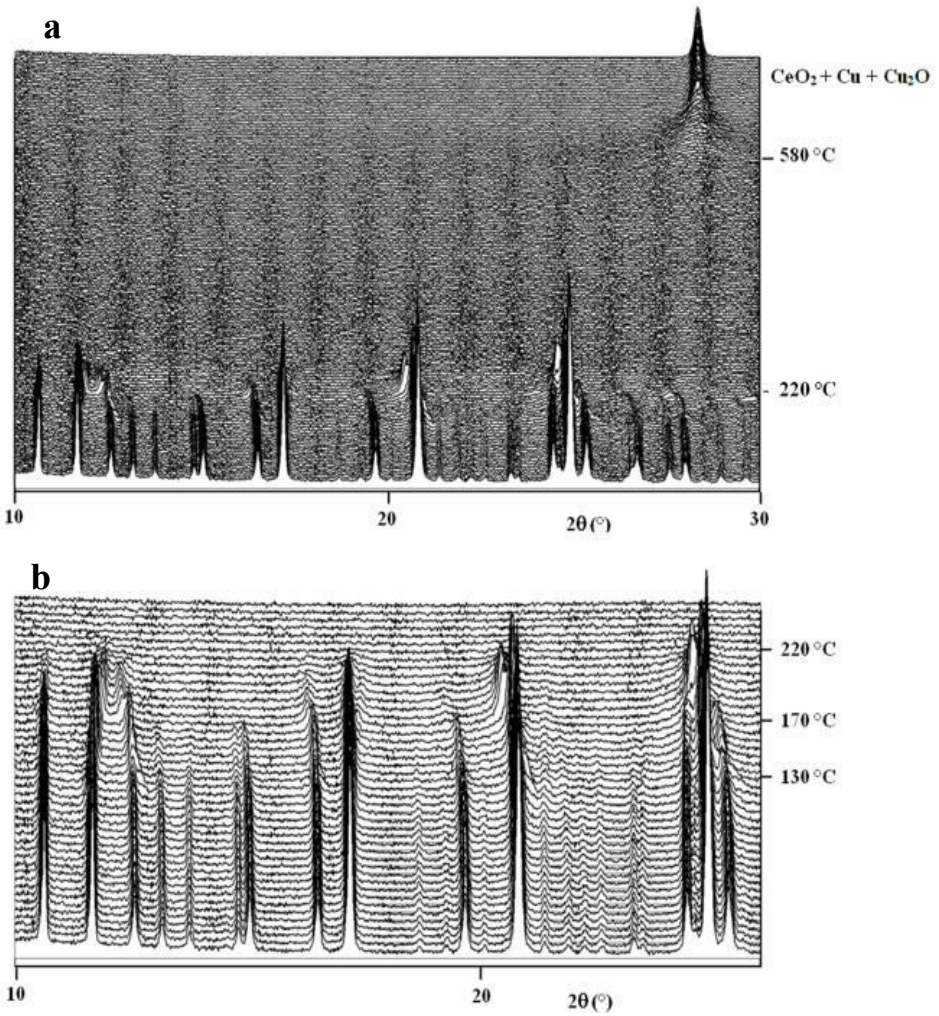

Figure 5

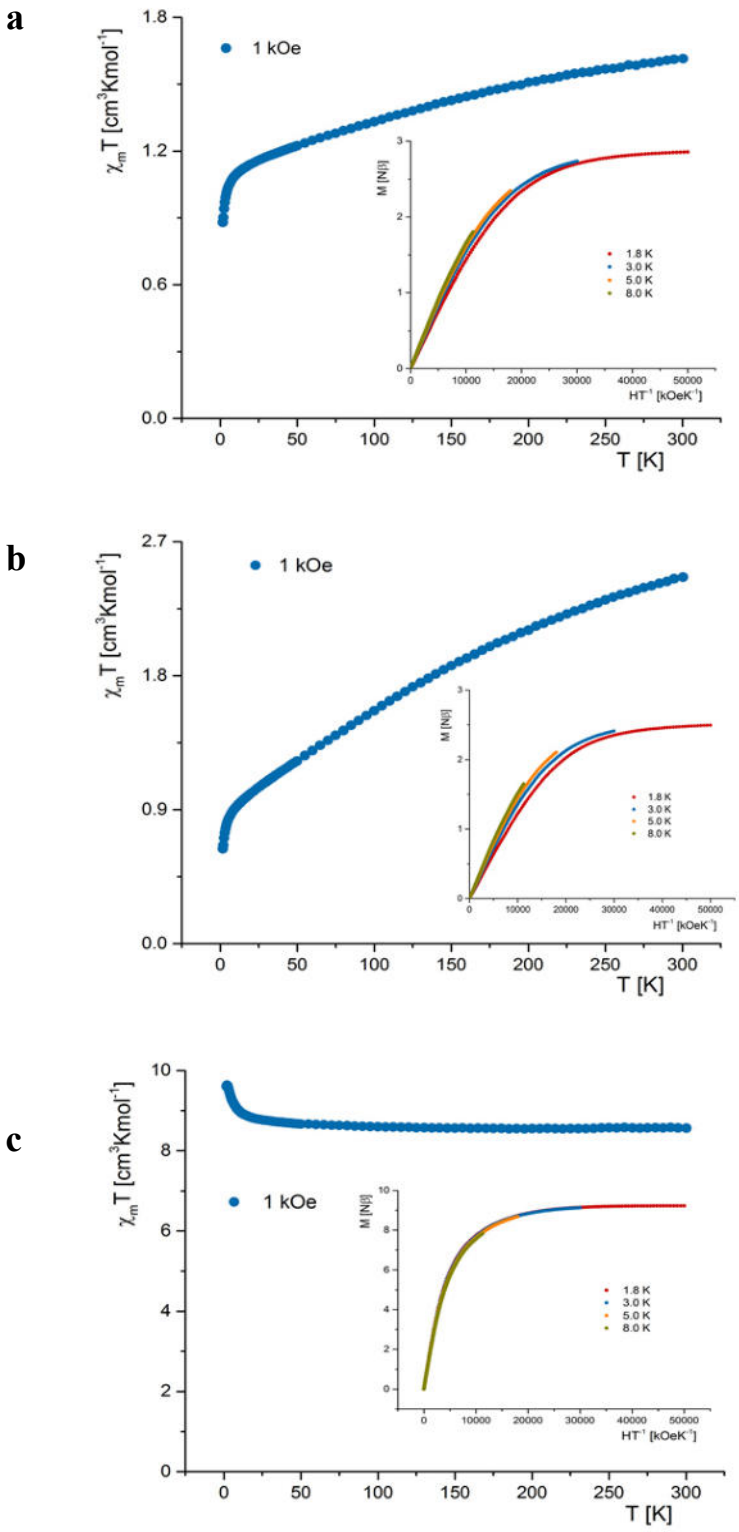

Figure 6

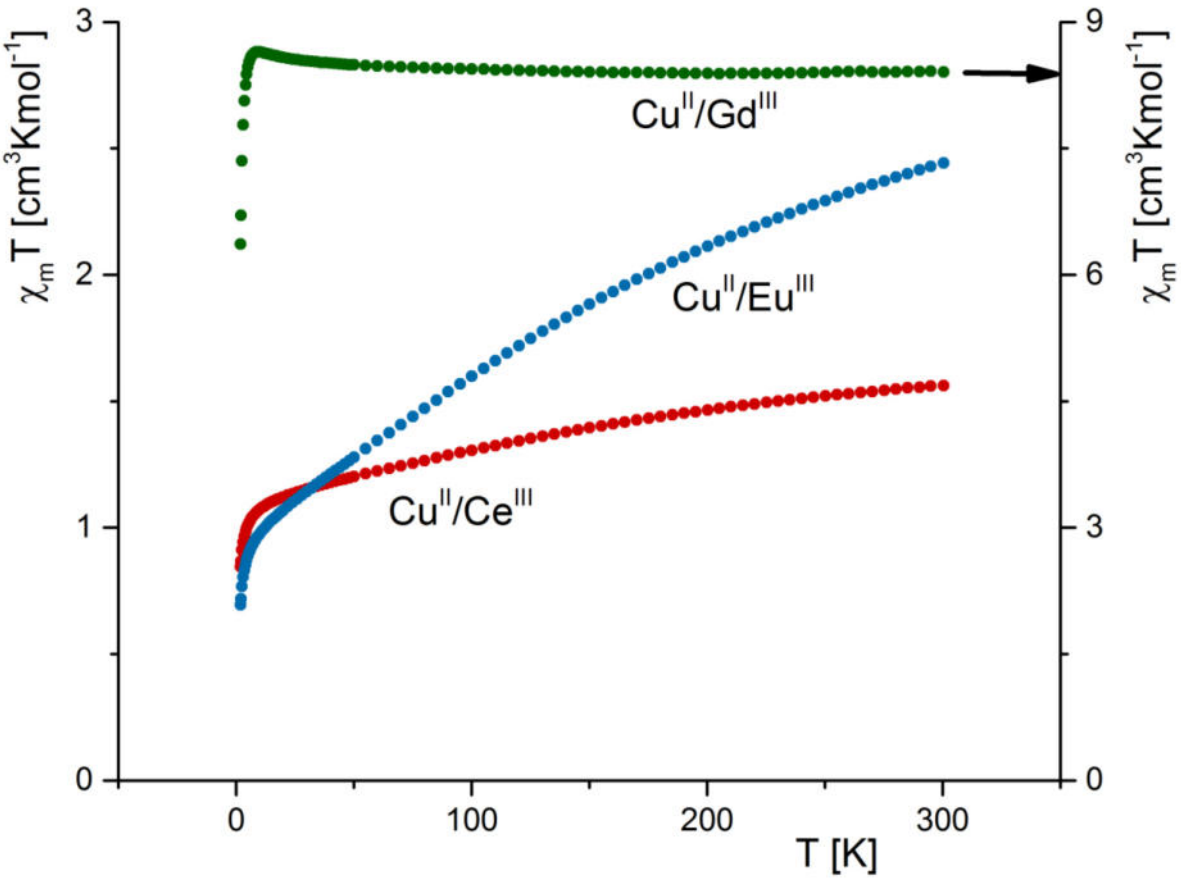

Figure 7

TABLES

Table 1. Crystal data details of (**1**), (**2**) and (**3**)

	$\{[Ln(DMF)_2(NO_3)Cu_2Cl_2(HIA)_4]\cdot(2DMF)\cdot(H_2O)\}_n$		
Formula	(**1**) Ln= Ce^{III}	(**2**) Ln=Eu^{III}	(**3**) Ln=Gd^{III}
Space group		$P3_221$	
Crystal system		Trigonal	
parameters (Å,°)	a=b=13.977(2), c= 22.773(2)	a=b=13.952(2), c= 22.836(4)	a=b=13.917(3), c= 22.8189(1)
Volume ($Å^3$)	3852.9(1)	3849.6(1)	3827.6(4)
Final R indexes [I>=2σ (I)]	R_1 = 0.0372, wR_2 = 0.0979	R_1 = 0.0449, wR_2 = 0.1116	R_1 = 0.0472, wR_2 = 0.1206
GooF	1.045	1.022	1.050
Flack parameter	0.46(3)	0.32(2)	0.48(3)

ASSOCIATED CONTENT

Supporting Information. The Supporting Information is available at https://..... Crystal data and refinement details, bond lengths, hydrogen bonds. Figure of the bridges. Channels observed in 3D-network. PXRD of the phases. Thermal analyses (TGA and PXRD diagrams). FTIR and UV-vis spectra. AC magnetic susceptibility and fits of $\chi_m T$ vs. T and M vs. H.

Codes CCDC 1910617, 1910618 and 1910619 contain the supplementary crystallographic data for this paper. These data can be obtained free of charge via www.ccdc.cam.ac.uk/data_request/cif, or by emailing data_ request@ccdc.cam.ac.uk, or by contacting The Cambridge Crystallographic Data Centre, 12 Union Road, Cambridge CB2 1EZ, UK; fax: +44 1223 336033.

AUTHOR INFORMATION

Corresponding Author

*Verónica Paredes-García, vparedes@unab.cl, +562 2661 5756; Nathalie Audebrand, nathalie.audebrand@univ-rennes1.fr, +332 2323 5714.

Author Contributions

The manuscript was written through the contributions of all authors. All authors have approved the final version of the manuscript.

ACKNOWLEDGMENT

The authors acknowledge FONDECYT 1170887 y 1211394, Proyecto Anillo CONICYT ACT 1404 grant, CONICYT-FONDEQUIP/PPMS/EQM130086, Chilean-French International Associated Laboratory for Multifunctional Molecules and Materials-LIA M3-CNRS N°1027 and

ECOS/CONICYT C15E02. Authors acknowledge CEDENNA, Financiamiento Basal, AFB 180001. BBH, thanks to postdoctoral project FONDECYT 3190436. The authors also acknowledge the support of the Laboratory of Analyses of Solids (L.A.S-UNAB) and the support of Guillaume Calvez from Laboratory ISCR/CSM-INSA, Rennes, France for optical measurements. B.B thanks CONICYT scholarship No 21140908 and Ecole Doctorale Science de la Matière (University of Rennes 1) for mobility grant. FEDER, Région Bretagne and Rennes Métropole contribute to the purchase of the in-situ X-Ray powder diffractometer in Rennes.

REFERENCES

[1] R. J. Kuppler, D. J. Timmons, Q.-R. Fang, J.-R. Li, T. A. Makal, M. D. Young, D. Yuan, D. Zhao, W. Zhuang, H.-C. Zhou. Potential applications of metal-organic frameworks. Coord. Chem. Rev. 253 (2009) 3042–3066. https://doi.org/10.1016/j.ccr.2009.05.019.

[2] S. Qiu, G. Zhu. Molecular engineering for synthesizing novel structures of metal-organic frameworks with multifunctional properties. Coord. Chem. Rev. 253 (2009) 2891-2911. https://doi.org/10.1016/j.ccr.2009.07.020.

[3] H.-C. Zhou, S. Kitagawa. Metal–Organic Frameworks (MOFs). Chem. Soc. Rev. 43 (2014) https://doi.org/10.1039//C4CS90059F.

[4] M. Schröder. Functional Metal-Organic Frameworks: Gas storage, Separation and Catalysis, Springer, Nottingham, 2010.

[5] D. Farrusseng. Metal-Organic Frameworks: Applications from Catalysis to Gas Storage, Wiley-VCH Verlag GmbH & Co., Weinheim, 2011.

[6] S. R. Batten, S. M. Neville, D. R. Turner. Coordination Polymers: Design, Analysis and Application, RSC Publishing, Cambridge, 2009.

[7] L. R. MacGillivray. Metal-Organic Frameworks: Design and Application, John Wiley & Sons, Inc., Hoboken, 2010.

[8] N. Stock, S. Biswas. Synthesis of Metal-Organic Frameworks (MOFs): Routes to Various MOF Topologies, Morphologies, and Composites. Chem. Rev. 112 (2012) 933-969. https://doi.org/10.1021/cr200304e.

[9] Y.-R. Lee, J. Kim, W.-S. Ahn. Synthesis of metal-organic frameworks: A mini review. Korean J. Chem. Eng. 30 (2013) 1667-1680. https://doi.org/10.1007/s11814-013-0140-6.

[10] V.V. Butova, M. A. Soldatov, A. A. Guda, K. A. Lomachenko, C. Lamberti, Metal-organic frameworks: structure, properties, methods of synthesis, and characterization. Russ. Chem. Rev. 85(3) (2016) 280-307. https://doi.org/10.1070/RCR4554.

[11] N. A. Khan, S. H. Jhung. Synthesis of metal-organic frameworks (MOFs) with microwave or ultrasound: Rapid reaction, phase-selectivity, and size reduction. Coord. Chem. Rev. 285 (2015) 11–23. https://doi.org/10.1016/j.ccr.2014.10.008.

[12] J. H. Bang, K. S. Suslick. Applications of Ultrasound to the Synthesis of Nanostructured Materials. Adv. Mater. 22 (2010) 1039–1059. https://doi.org/10.1002/adma.200904093.

[13] J.-L. Luche. Synthetic Organic Sonochemistry, Springer Science, Bussiness Media, New York, 1998.

[14] P. W. Cains, P. D. Martin, C. J. Price. The Use of Ultrasound in Industrial Chemical Synthesis and Crystallization. 1. Applications to Synthetic Chemistry. Org. Process Res. Dev. 2 (1998) 34–48. https://doi.org/10.1021/op9700340.

[15] V. Safarifard, A. Morsali. Applications of ultrasound to the synthesis of nanoscale metal–organic coordination polymers. Coord. Chem. Rev. 292 (2015) 1-14. https://doi.org/10.1016/j.ccr.2015.02.014.

[16] G. Sargazia, D. Afzali, N. Daldosso, H. Kazemian, N. Chauhan, Z. Sadeghian, T. Tajerian, A. Ghafarinazari, M. Mozafari. A systematic study on the use of ultrasound energy for the synthesis of nickel–metal organic framework compounds. Ultrason. Sonochem. 27 (2015) 395-402. https://doi.org/10.1016/j.ultsonch.2015.04.004.

[17] L.-G. Qiu, Z.-Q. Li, Y. Wu, W. Wang, T. Xua, X. Jiang. Facile synthesis of nanocrystals of a microporous metal–organic framework by an ultrasonic method and selective sensing of organoamines. Chem. Commun. (2008) 3642-3644. https://doi.org/10.1039/B804126A.

[18] Z.-Q. Li, L.-G. Qiu, W. Wang, T. Xu, Y. Wu, X. Jiang. Fabrication of nanosheets of a fluorescent metal–organic framework $[Zn(BDC)(H_2O)]_n$ (BDC = 1,4-benzenedicarboxylate): Ultrasonic synthesis and sensing of ethylamine. Inorg. Chem. Commun. 11 (2008) 1375–1377. https://doi.org/10.1016/j.inoche.2008.09.010.

[19] R. Li, Y.-P. Yuan, L.-G. Qiu, W. Zhang, J.-F. Zhu. A Rational Self- Sacrificing Template Route to Metal–Organic Framework Nanotubes and Reversible Vapor- Phase

Detection of Nitroaromatic Explosives. Small. 8 (2012) 225-230. https://doi.org/10.1002/smll.201101699.

[20] S. Shamaei, A. R. Abbasi, N. Noori, E. Rafiee, A. Azadbakht. Ultrasound-assisted coating of silk yarn with nano-porous $Co_3(BTC)_2 \cdot 12H_2O$ with iodine adsorption affinity Colloids Surf. A. 431 (2013) 66-72. https://doi.org/10.1016/j.colsurfa.2013.04.036.

[21] N. A. Khan, M. M.Haque, S. H. Jhung. Accelerated Syntheses of Porous Isostructural Lanthanide–Benzenetricarboxylates (Ln–BTC) Under Ultrasound at Room Temperature. Eur. J. Inorg. Chem. 31 (2010) 4975-4981. https://doi.org/10.1002/ejic.201000541.

[22] K. Liu, H. You, G. Jia, Y. Zheng, Y. Huang, Y. Song, M. Yang, L. Zhang, H. Zhang. Hierarchically Nanostructured Coordination Polymer: Facile and Rapid Fabrication and Tunable Morphologies. Cryst. Growth Des. 2010, 10, 790-797. https://doi.org/10.1021/cg901170j.

[23] R. J. Pearson. Hard and Soft Acids and Bases. Am. Chem. Soc. 85 (1963) 3533-3539. https://doi.org/10.1021/ja00905a001.

[24] M. Barbatti. The role of tautomers in the UV absorption of urocanic acid. Phys. Chem. Chem. Phys. 13 (2011) 4686–4692. https://doi.org/10.1039/C0CP02142C.

[25] Y. Xu, J. Xi, W. Wei, Y. Chi, C. Hu. A 3D homochiral framework with rare $4^9 \cdot 6^6$ structural topology constructed by unique triple-stranded helices. Inorg. Chem. Commun. 13 (2010) 852-854. https://doi.org/10.1016/j.inoche.2010.04.011.

[26] R.-Q. Zou, R.-Q. Zhong, L. Jiang, Y. Yamada, N. Kuriyama, Q. Xu. Tuning the Formation of Cadmium(II) Urocanate Frameworks by Control of Reaction Conditions: Crystal Structure, Properties, and Theoretical Investigation. Chem. Asian J. 1 (2006) 536-543. https://doi.org/10.1002/asia.200600113.

[27] Bruker, APEX3 (V2016.1-0), Bruker AXS Inc., Madison, Wisconsin, USA, 2016.

[28] Sheldrick, G. M. SAINT (Version 8.37A), Bruker AXS Inc., Madison, Wisconsin, USA, 2016.

[29] Sheldrick, G. M. SADABS (Version 2014/15), Bruker AXS Inc., Madison, Wisconsin, USA, 2014.

[30] G. M. Sheldrick. SHELXT - Integrated space-group and crystal-structure determination. Acta Crystallogr. Sect. A. A71(2015) 3–8. https://doi.org/10.1107/S2053273314026370.

[31] G. M. Sheldrick. Crystal structure refinement with SHELXL. Acta Crystallogr., Sect. C. C71 (2015) 3–8. https://doi.org/10.1107/S2053229614024218.

[32] O. V. Dolomanov, L. J. Bourhis, R. J. Gildea, J. A. K. Howard, H. Puschmann. OLEX2: a complete structure solution, refinement and analysis program. J. Appl. Crystallogr., 42 (2009) 339–341. https://doi.org/10.1107/S0021889808042726.

[33] K. Brandenburg. DIAMOND (Version 4.4.1), Crystal Impact GbR Bonn, Germany, 2017.

[34] L. J. Farrugia. WinGX and ORTEP for Windows: an update. J. Appl. Crystallogr. 45 (2012) 849-854. https://doi.org/10.1107/S0021889812029111.

[35] M. Llunell, D. Casanova, J. Cirera, J. Bofill, P. Alemany, S. Alvarez, M. Pinsky, D. Avnir. SHAPE (V2.1), Universitat de Barcelona, Barcelona, 2013.

[36] G. Bain,; J. Berry. Diamagnetic Corrections and Pascal's Constants. J. Chem. Educ. 85 (2008) 532-536. https://doi.org/10.1021/ed085p532.

[37] R.-Q. Fan, P. Wang, Y.-L. Yang, Y.-J. Zhang, Y.-B. Yin, W. Hasi. Syntheses, structures, and luminescent properties of copper(II) complexes based on 2,6-bis(imino)pyridyl ligands. Polyhedron. 29 (2010) 2862–2866. https://doi.org/10.1016/j.poly.2010.07.012.

[38] O. Iasco, G. Novitchi, E. Jeanneau, W. Wernsdorfer, D. Luneau. Benzoxazole-Based Heterometallic Dodecanuclear Complex [$Dy^{III}_4Cu^{II}_8$] with Single-Molecule-Magnet Behavior. Inorg. Chem. 50 (2011) 7373–7375. https://doi.org/10.1021/ic201070n.

[39] F. He, M.-L. Tong, X.-L. Yu, X.-M. Chen. Controlled Aggregation of Heterometallic Nanoscale $Cu_{12}Ln_6$ Clusters (Ln = Gd^{III} or Nd^{III}) into 2D Coordination Polymers. Inorg. Chem. 44 (2005) 559-565. https://doi.org/10.1021/ic048754s.

[40] F. Chen, W. Lu, Y. Zhu, B. Wu, X. Zheng. Syntheses, crystal structures, and magnetic properties of RE(III)–Cu(II) heteronuclear complexes with α-methylacrylic acid. J. Coord. Chem. 63 (2010) 3599–3609. https://doi.org/10.1080/00958972.2010.514904.

[41] Y.-H. Liu, H.-Ch. Wu, H.-M. Lin, W.-H. Hou, K.-L. Lu. Crystal engineering toward intersecting channels in an interpenetrated diamondoid network based on a net-to-net H-bonding interaction. Chem. Commun. (2003) 60–61. https://doi.org/10.1039/B208683B.

[42] X. Feng, Y.-H. Wen, Y.-Z. Lan, Y.-L. Feng, C.-Y. Pan Y.-G. Yao. Multifunctional zinc(II) urocanate with rare fivefold interpenetrating diamondoid network. Inorg. Chem. Commun. 12 (2009) 89-91. https://doi.org/10.1016/j.inoche.2008.11.017.

[43] R.-Q. Zou, Y. Yamada, Q. Xu. Strong fluorescent emission of a new fourfold-interpenetrated diamondoid metal-organic framework of zinc(II) urocanate with one-dimensional open channels. Microporous Mesoporous. Mater. 91 (2006) 233–237. https://doi.org/10.1016/j.micromeso.2005.11.048.

[44] C. R. Groom, I. J. Bruno, M. P. Lightfoot, S. C. Ward. The Cambridge Structural Database. Acta Crystallogr. Sect. B. B72 (2016) 171-179. http://dx.doi.org/10.1107/S2052520616003954.

[45] E. J. Baran, E. G. Ferrer, C. I. Muglia. Kristallstruktur, Schwingungsspektren und thermisches Verhalten der Cobalt(II)- und Zink(II)- Komplexe der Urocaninsäure. Z. Anorg. Allg. Chem. 623 (1997) 316-323. https://doi.org/10.1002/zaac.19976230151.

[46] M. A. Ali, D.A. Chowdhury-I, M. N. Uddin. Four- and five-coordinate copper(II) complexes containing mixed ligands. Polyhedron 3 (1984) 595-598. https://doi.org/10.1016/S0277-5387(00)88093-6.

[47] M. A. Ali, S.E. Livingstone, D. J. Phillips. Metal chelates of dithiocarbazic acid and its derivatives. VII. The magnetism of some copper(II) complexes of salicylaldehyde Schiff bases derived from N-methyl-S-methyldithiocarbazate and S,S′-dimethyldithiocarbazate. Inorg. Chim. Acta, 7 (1973) 531-537. https://doi.org/10.1016/S0020-1693(00)94878-3.

[48] E. Espada-Bellido, M. Galindo-Riaño, M. García-Vargas, R. Narayanaswamy. Selective Chemosensor for Copper Ions Based on Fluorescence Quenching of a Schiff-Base Fluorophore. Appl. Spectrosc. 64 (2010) 727-732. https://doi.org/10.1366/000370210791666282.

[49] M. Hazra, T. Dolai, A. Pandey, S. Kumar, A. Patra. Fluorescent copper(II) complexes: The electron transfer mechanism, interaction with bovine serum albumin (BSA) and antibacterial activity. J. Saudi Chem. Soc. 21 (2017) S240-S247. https://doi.org/10.1016/j.jscs.2014.02.009.

[50] C. Benelli, D. Gatteschi. Introduction to Molecular Magnetism From Transition Metals to Lanthanides. Wiley-VCH Verlag GmbH & Co. KGaA, Germany, 2015.

[51] X-J. Song, Z-C. Zhang, Y.-L. Xu, J. Wang, H-B. Zhou, Y. Song. Assembling 1D magnetic chain based on octacyanotungstate(v) and [Cu_2L_2Ln] sub-building units (Ln = Eu, Gd, Tb and Dy). Dalton Trans. 42 (2013) 9505-9512. https://doi.org/10.1039/C3DT50173F.

[52] M. Atzori, S. Benmansour, G. Mínguez, M. Clemente-León, A. Abhervé, P. Gómez-Claramunt, E. Coronado, F. Artizzu, E. Sessini, P. Deplano, A. Serpe, M.-L.

Mercuri, C. Gómez. A Family of Layered Chiral Porous Magnets Exhibiting Tunable Ordering Temperatures. Inorg. Chem. 52 (2013) 10031–10040. https://doi.org/10.1021/ic4013284.

[53] J. Li, B. Li, P. Huang, H.-Y. Shi, R.-B. Huang, L.-S. Zheng, J. Tao. Four Coordination Polymers Based on Identical Eight-Connected Heptanuclear Clusters: Spin Canting, Spin Glass, Antiferromagnetism, and Gas Adsorption. Inorg. Chem. 52 (2013) 11573–11579. https://doi.org/10.1021/ic401912k.

[54] M. Andruh, J.-P. Costes, C. Diaz, S. Gao. 3d−4f Combined Chemistry: Synthetic Strategies and Magnetic Properties. Inorg. Chem., 2009, 48, 3342–3359. https://doi.org/10.1021/ic801027q.

[55] C. Landee, M. Turnbull. Review: A gentle introduction to magnetism: units, fields, theory, and experiment. J. Coord. Chem. 67 (2014) 375–439. https://doi.org/10.1080/00958972.2014.889294.

[56] A. Madalan, N. Avarvari, M. Fourmigué, R. Clérac, L. Chibotaru, S. Clima, M. Andruh. Heterospin Systems Constructed from $[Cu_2Ln]^{3+}$ and $[Ni(mnt)_2]^{1-,2-}$ Tectons: First 3p−3d−4f Complexes (mnt = Maleonitriledithiolato). Inorg. Chem., 47 (2008) 940–950. https://doi.org/10.1021/ic701738z.

[57] T. Shiga, M. Ohba, H. Ōkawa. A Series of Trinuclear $Cu^{II}Ln^{III}Cu^{II}$ Complexes Derived from 2,6-Di(acetoacetyl)pyridine: Synthesis, Structure, and Magnetism. Inorg. Chem., 43 (2004) 4435–4446. https://doi.org/10.1021/ic034998l.

[58] M. Kahn, C. Mathonière, O. Kahn. Nature of the Interaction between Ln^{III} and Cu^{II} Ions in the Ladder-Type Compounds $\{Ln_2[Cu(opba)]_3\}\cdot S$ (Ln = Lanthanide Element; opba = ortho-Phenylenebis(oxamato), S = Solvent Molecules). Inorg. Chem. 38 (1999) 3692–3697. https://doi.org/10.1021/ic9811998.